Ultra-thin broadband nanostructured insulator-metal-insulator-metal plasmonic light absorber

Aliaksandr Hubarevich,[1] Aliaksandr Kukhta,[2] Hilmi Volkan Demir,[1] Xiaowei Sun,[1,3] and Hong Wang[1,*]

[1]*School of Electrical and Electronic Engineering, Nanyang Technological University, 50 Nanyang Avenue, 639798, Singapore*

[2]*Institute for Nuclear Problems, Belarusian State University, 11 Bobruiskaya Str., Minsk, 220050, Belarus*

[3]*EXWSUN@ntu.edu.sg*

[*]*EWANGHONG@ntu.edu.sg*

Abstract: An ultra-thin nanostructured plasmonic light absorber with an insulator-metal-insulator-metal (IMIM) architecture is designed and numerically studied. The IMIM structure is capable to absorb up to about 82.5% of visible light in a broad wavelength range of 300-750 nm. The absorption by the bottom metal is only 6% of that of the top metal. The results show that the IMIM architecture has weak dependence of the angle of the incident light. Interestingly, by varying the top insulator material the optical absorption spectrum can be shifted more than 180 nm as compared to the conventional *air*-metal-insulator-metal structure. The IMIM structure can be applied for different plasmonic devices with improved performance.

OCIS codes: (310.3915) Metallic, opaque, and absorbing coatings; (160.4236) Nanomaterials.

References and links

1. S. Chhajed, M. F. Schubert, J. K. Kim, and E. F. Schubert, "Nanostructured multilayer graded-index antireflection coating for Si solar cells with broadband and omnidirectional characteristics," Appl. Phys. Lett. **93**(25), 251108 (2008).
2. D. Bouhafs, A. Moussi, A. Chikouche, and J. Ruiz, "Design and simulation of antireflection coating systems for optoelectronic devices: Application to silicon solar cells," Sol. Energy Mater. Sol. Cells **52**(1-2), 79–93 (1998).
3. K.-Q. Peng, X. Wang, L. Li, X.-L. Wu, and S.-T. Lee, "High-performance silicon nanohole solar cells," J. Am. Chem. Soc. **132**(20), 6872–6873 (2010).
4. S. E. Han and G. Chen, "Optical absorption enhancement in silicon nanohole arrays for solar photovoltaics," Nano Lett. **10**(3), 1012–1015 (2010).
5. F. Wang, H. Yu, J. Li, X. Sun, X. Wang, and H. Zheng, "Optical absorption enhancement in nanopore textured-silicon thin film for photovoltaic application," Opt. Lett. **35**(1), 40–42 (2010).
6. J. Li, H. Yu, and Y. Li, "Aligned Si nanowire-based solar cells," Nanoscale **3**(12), 4888–4900 (2011).
7. L. Tsakalakos, J. Balch, J. Fronheiser, B. Korevaar, O. Sulima, and J. Rand, "Silicon nanowire solar cells," Appl. Phys. Lett. **91**(23), 233117 (2007).
8. S. Jeong, E. C. Garnett, S. Wang, Z. Yu, S. Fan, M. L. Brongersma, M. D. McGehee, and Y. Cui, "Hybrid silicon nanocone-polymer solar cells," Nano Lett. **12**(6), 2971–2976 (2012).
9. K. X. Wang, Z. Yu, V. Liu, Y. Cui, and S. Fan, "Absorption enhancement in ultrathin crystalline silicon solar cells with antireflection and light-trapping nanocone gratings," Nano Lett. **12**(3), 1616–1619 (2012).
10. J. Li, H. Yu, Y. Li, F. Wang, M. Yang, and S. M. Wong, "Low aspect-ratio hemispherical nanopit surface texturing for enhancing light absorption in crystalline Si thin film-based solar cells," Appl. Phys. Lett. **98**(2), 021905 (2011).
11. H. A. Atwater and A. Polman, "Plasmonics for improved photovoltaic devices," Nat. Mater. **9**(3), 205–213 (2010).
12. S. Pillai, K. Catchpole, T. Trupke, and M. Green, "Surface plasmon enhanced silicon solar cells," J. Appl. Phys. **101**(9), 093105 (2007).
13. V. E. Ferry, M. A. Verschuuren, H. B. Li, E. Verhagen, R. J. Walters, R. E. Schropp, H. A. Atwater, and A. Polman, "Light trapping in ultrathin plasmonic solar cells," Opt. Express **18**(S2 Suppl 2), A237–A245 (2010).
14. Q. Liang, W. Yu, W. Zhao, T. Wang, J. Zhao, H. Zhang, and S. Tao, "Numerical study of the meta-nanopyramid array as efficient solar energy absorber," Opt. Mater. Express **3**(8), 1187–1196 (2013).
15. M. Lobet, M. Lard, M. Sarrazin, O. Deparis, and L. Henrard, "Plasmon hybridization in pyramidal metamaterials: a route towards ultra-broadband absorption," Opt. Express **22**(10), 12678–12690 (2014).

#232636 - $15.00 USD Received 16 Jan 2015; revised 1 Mar 2015; accepted 30 Mar 2015; published 8 Apr 2015

16. M. K. Hedayati, F. Faupel, and M. Elbahri, "Tunable broadband plasmonic perfect absorber at visible frequency," Appl. Phys., A Mater. Sci. Process. **109**(4), 769–773 (2012).
17. Y. Cui, K. H. Fung, J. Xu, S. He, and N. X. Fang, "Multiband plasmonic absorber based on transverse phase resonances," Opt. Express **20**(16), 17552–17559 (2012).
18. A. Manjavacas, J. G. Liu, V. Kulkarni, and P. Nordlander, "Plasmon-induced hot carriers in metallic nanoparticles," ACS Nano **8**(8), 7630–7638 (2014).
19. F. Wang and N. A. Melosh, "Plasmonic energy collection through hot carrier extraction," Nano Lett. **11**(12), 5426–5430 (2011).
20. S. Mubeen, J. Lee, W.-R. Lee, N. Singh, G. D. Stucky, and M. Moskovits, "On the plasmonic photovoltaic," ACS Nano **8**(6), 6066–6073 (2014).
21. T. Gong and J. N. Munday, "Angle-independent hot carrier generation and collection using transparent conducting oxides," Nano Lett. **15**(1), 147–152 (2015).
22. H. Chalabi, D. Schoen, and M. L. Brongersma, "Hot-electron photodetection with a plasmonic nanostripe antenna," Nano Lett. **14**(3), 1374–1380 (2014).
23. W. Li and J. Valentine, "Metamaterial perfect absorber based hot electron photodetection," Nano Lett. **14**(6), 3510–3514 (2014).
24. K. Aydin, V. E. Ferry, R. M. Briggs, and H. A. Atwater, "Broadband polarization-independent resonant light absorption using ultrathin plasmonic super absorbers," Nat. Commun. **2**, 517 (2011).
25. A. Li, F. Muller, A. Birner, K. Nielsch, and U. Gosele, "Hexagonal pore arrays with a 50-420 nm interpore distance formed by self-organization in anodic alumina," J. Appl. Phys. **84**(11), 6023–6026 (1998).
26. K. Yasui, K. Nishio, H. Nunokawa, and H. Masuda, "Ideally ordered anodic porous alumina with sub-50 nm hole intervals based on imprinting using metal molds," J. Vac. Sci. Technol. B **23**(4), L9–L12 (2005).
27. S. Chu, K. Wada, S. Inoue, M. Isogai, Y. Katsuta, and A. Yasumori, "Large-scale fabrication of ordered nanoporous alumina films with arbitrary pore intervals by critical-potential anodization," J. Electrochem. Soc. **153**(9), B384–B391 (2006).
28. G. Ghosh, *Handbook of Optical Constants of Solids: Handbook of Thermo-Optic Coefficients of Optical Materials with Applications* (Academic, 1998).
29. Y.-H. Ye and J.-Y. Zhang, "Enhanced light transmission through cascaded metal films perforated with periodic hole arrays," Opt. Lett. **30**(12), 1521–1523 (2005).
30. M. Rycenga, C. M. Cobley, J. Zeng, W. Li, C. H. Moran, Q. Zhang, D. Qin, and Y. Xia, "Controlling the synthesis and assembly of silver nanostructures for plasmonic applications," Chem. Rev. **111**(6), 3669–3712 (2011).
31. D. Chanda, K. Shigeta, T. Truong, E. Lui, A. Mihi, M. Schulmerich, P. V. Braun, R. Bhargava, and J. A. Rogers, "Coupling of plasmonic and optical cavity modes in quasi-three-dimensional plasmonic crystals," Nat. Commun. **2**, 479 (2011).
32. B. Huttner, "Optical properties of polyvalent metals in the solid and liquid state: aluminum," J. Phys. Condens. Matter **6**(13), 2459–2474 (1994).
33. Lumerical FDTD Solutions, *https://www.lumerical.com/tcad-products/fdtd/*.

1. Introduction

Photovoltaic (PV) technologies based on direct conversion of the solar energy into electricity are being continuously developed and commercialized. The main optical process taking place in PV devices is light absorption and it is one of the limiting factors in thin film PV cells. Approaches to enhance absorption based on fabrication of antireflection coatings [1, 2], nanoholes [3–5], nanowires [6, 7], nanocones [8, 9] and other inhomogeneities [10] have been successfully studied and applied. In recent years, plasmonic metallic nanostructures are found to be an effective means as well [11–18]. The plasmonic nanostructures scatter incident light and increase the photon path length in the absorbed layer. Moreover, the strong local field enhancement around the metal inhomogeneities results in an increase of absorption in a surrounding semiconductor.

Interestingly, plasmonic metal-insulator-metal (MIM) structures themselves can be used as a hot electron PV device [19–23]. The operation of these devices relies on the hot electrons absorbed in metallic nanostructures by surface plasmon resonance. The properties of these resonances are determined by the metal material, its environment, the size and shape of the nanostructure. In such plasmonic PV devices, light is preferentially absorbed by one metal layer, exciting hot electrons in the metal, which can then tunnel to the counter metal layer generating current. Obviously, the performance of this plasmonic PV device is determined by the metal layer absorption and the absorption difference of the two metal layers. An average absorption of 71% in the visible range (400-700 nm) has been recently achieved using a metal

#232636 - $15.00 USD Received 16 Jan 2015; revised 1 Mar 2015; accepted 30 Mar 2015; published 8 Apr 2015

trapezoid array grating made of a MIM structure with a total device thickness of less than 200 nm [24]. In this paper, we design a new polarization-independent nanopatterned light trapping structure made of an ultra-thin insulator-metal-insulator-metal (IMIM) architecture. Compared to the MIM structures the IMIM design allows us to archive higher absorption up to 82.5% in a broad wavelength range from 300 to 750 nm. More importantly, the use of additional top dielectric provides the freedom to shift the absorption spectrum catering for different applications.

2. Materials, structures and simulation methods

The schematic diagram of the IMIM structure with both slanted and cross-sectional views is shown in Fig. 1. The structure can be fabricated by a simple process flow with one step lithography using hydrogen silsesquioxane (HSQ) in conjunction with metal and insulator depositions as illustrated in Fig. 1(b). Compared to the conventional MIM structures, an insulator is added on the top metal. The aluminum (*Al*) has been chosen as the bottom metal layer owing to its high reflectivity resulting in near zero light transmission in such structures [32].

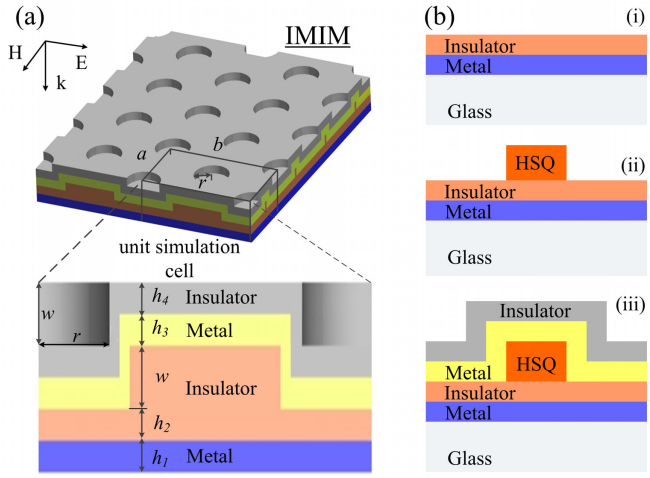

Fig. 1. (a) Schematic diagram (top) and cross-section of simulation unit cell (bottom) of IMIM structure. In the figure a, r, w, h_1, $(h_2 + w)$, h_3 and h_4 are interpore distance, pore radius, pore depth, bottom metal thickness, bottom insulator thickness, top metal thickness and top insulator thickness respectively. (b) Fabrication of IMIM structure on a glass substrate. (i) Deposition of *Al* on glass followed by atomic layer deposition (ALD) of Al_2O_3 with thickness of h_2; (ii) Formation of SiO_2 mesa with thickness of w using HSQ by lithography and curing; (iii) Deposition of top metal and insulator to form the IMIM structure with thickness of h_3 and h_4 respectively.

The hexagonal pores arrangement and aluminum oxide (Al_2O_3) bottom insulator layer were chosen due to easily formation of hexagonal porous Al_2O_3 by electrochemical anodization of *Al* [25–27]. Of course, the same design can also be fabricated by using conventional micro-fabrication technologies. Gold (*Au*), silver (*Ag*) and copper (*Cu*) exhibit the highest plasmonic response (sensitivity) and hence they are used as material for the top metal layer. Different top insulator layers including Si_3N_4, Al_2O_3, SiO_2 and MgF_2 with averaged values of refraction index in the visible region of 2.5, 1.8, 1.54 and 1.38 respectively were evaluated [28].

The designed structures were analyzed under the framework of full-field electromagnetic simulations based on numerical solution of time-dependent Maxwell equations using the finite-difference time-domain (FDTD) method, which is available from Lumerical software package [33]. Similar approach has been successfully used in predicting the resonance peak

#232636 - $15.00 USD Received 16 Jan 2015; revised 1 Mar 2015; accepted 30 Mar 2015; published 8 Apr 2015

positions and the absorption spectrum of a MIM structure [24]. The periodic boundary condition along the vertical axes and perfectly matched layers along the horizontal axis with a normal incident plane wave excitation are applied. The calculation mesh size is 2 nm in all directions. The absorption spectrum in the range of 200-800 nm is calculated for different structures, and the averaged absorption is determined for the range of 300-750 nm. In order to obtain two-dimensional absorption profile G, a simple expression has been used $G = -1/2\,\omega\varepsilon''|E|^2$, where ε'' is the imaginary part of material permittivity, ω is the angular frequency, and $|E|^2$ is the electric field intensity [33].

3. Results and discussion

The impact of geometrical parameters such length, width and thickness, etc. on the absorption is simulated for structure optimization. The thickness of metals is chosen according to metal plasmon skin depth, which is given by Eq. (1) [29]:

$$\delta = \frac{c}{\omega \operatorname{Im}\sqrt{\varepsilon_m}}, \tag{1}$$

where ε_m, ω and c are imaginary values of metal dielectric constant, angular frequency of light and speed of light, respectively. For example, for wavelength range of 200-800 nm, the plasmon skin depth of gold varies from 5 to 25 nm correspondingly. Therefore, the thickness of 25 nm is enough for the comprehensive (maximum) absorption simulation of the *Au* layers. The pore diameter, ranging from 10 to 100 nm, interpore distance of 250-500 nm range and pore depth of 5-175 nm range were selected for IMIM design optimization following the optimized design of the MIM structure [24].

Figure 2(a) demonstrates the influence of pore depth w variations on the absorption IMIM structure. The parameters of r, a and $h_1 = h_2 = h_3 = h_4$ were chosen to 80, 320 and 25 nm respectively. The IMIM structure used for calculations contains Si_3N_4-Au-Al_2O_3-Al layers correspondingly. Considering the high absorption and large wavelength range of absorption spectrum as the figure-of-merit for the design of IMIM absorber, Fig. 2(a) suggests that the pore depth in range of 60-80 nm could provide higher absorption with wider absorption spectrum. Therefore, in following discussion w of 75 nm will be used for analyses. The influence of w on the absorption and its underlying mechanism, the effects of two types of surface plasmon resonance: localized surface plasmons (LSPs) and surface plasmon polaritons (SPPs) should be considered. The absorption caused by LSPs should occur at metal surface limited by a distance between any nearest two pores, while SPPs cover a distance of three or more pores located within the same direction and provoke the absorption close to the pores and inside them. For the shallow pores with depth w below 50 nm, the absorption is mainly induced by LSPs in the wavelength range of 250 to 500 nm. The increase in w up to100 nm may expand the absorption spectrum range up to 650 nm, which could be attributed to the contribution from SPPs. Further increase in the depth of the pores will weaken the SPPs related absorption resulting in the decrease of absorption at the bottom part of the pores. As to the pore radius, it is seen from Fig. 2(b) that the highest absorption can be obtained, when r

#232636 - $15.00 USD Received 16 Jan 2015; revised 1 Mar 2015; accepted 30 Mar 2015; published 8 Apr 2015

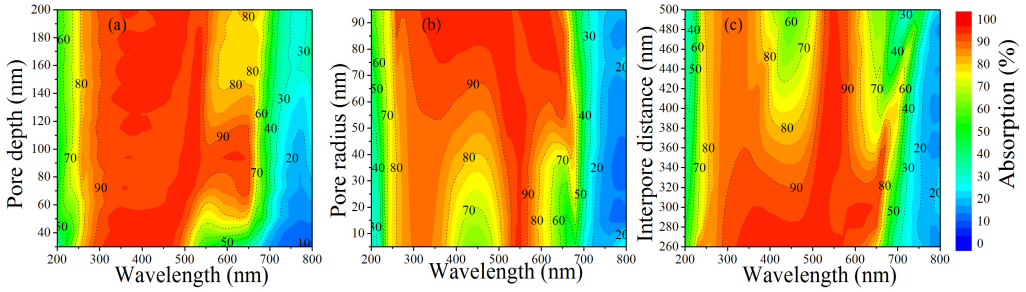

Fig. 2. The influence of pore depth *w* (a), pore radius *r* (b) and interpore distance *a* (c) variations on the absorption of the Si_3N_4-*Au*-Al_2O_3-*Al* (IMIM) structure.

is designed in the range of 60 to 100 nm. The ratio of *r* to *d* between two pores is in the range of 40-60%. Use *r* of 75 nm would provide sufficient process margin for the fabrication. The absorption peaked at 320 nm is related to LSPs, while the second absorption peak at 540 nm is attributed to SPPs related absorption. By changing interpore distance *d*, the absorption was calculated as shown in Fig. 2(c). An optimal *d* of 300 nm provides more 90% absorption with large spectrum range. For an interpore distance larger than 360 nm, the absorption peak at shorter wavelength (~310 nm) is due to LSPs related absorption, and the peak at 550 nm is contributed from SPPs related absorption.

The simulation shows that the absorption is largely affected by the top metal and top insulator layers. They are critical for the optimization of IMIM structure. Figures 3(a) and 3(b) show the influence of the thickness and material of the top metal layer on absorption. Indeed, a metal thickness larger than 20 nm is required, which is predicted by Eq. (1). It is interesting to note that *Ag* has poorer result in comparison to *Au* and *Cu*, which is could be due to the higher plasmonic strength for *Ag* at Si_3N_4/*Ag* interface in comparison to *Cu* and *Au* [30]. Figures 3(c) and 3(d) illustrate the influence of the thickness and material of the top insulator layer on absorption. The variation of Si_3N_4 layer thickness significantly affects both absorption and its wavelength range. It is can be seen that change of top insulator shifts the plasmon resonance modes. The insulator of higher reflective index moves plasmon response to longer wavelength. The Si_3N_4 layer shifts plasmon response for 180 nm in comparison to *air* (vacuum) [Fig. 3(e)]. This phenomenon can be explained by changing the interaction between electrons in metal and incident light, which is strongly dependent on its dielectric-surrounding medium. Surprisingly, the material of bottom insulator only slightly changes the absorption of IMIM structure [Fig. 3(f)]. This can be explained by the low transmission thought the top metal layer. Because ~70% of light has been absorbed by the top metal layer [it can be seen in Fig. 4(c)]. Only 10% of light can reach the bottom metal layer. Therefore, the effect of bottom insulator to the absorption of the IMIM structure is insignificant.

#232636 - $15.00 USD Received 16 Jan 2015; revised 1 Mar 2015; accepted 30 Mar 2015; published 8 Apr 2015

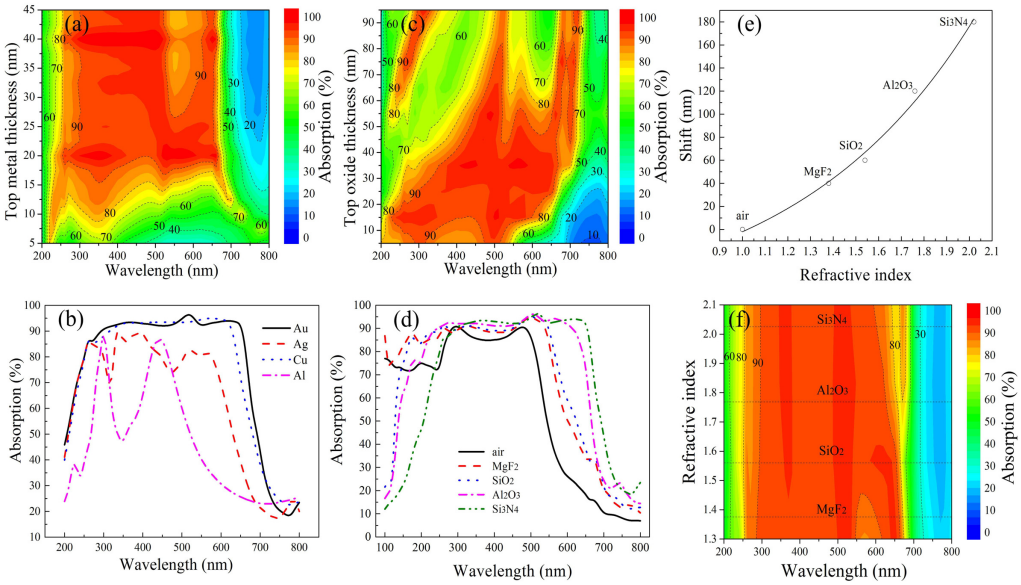

Fig. 3. Thickness and material type dependency on the absorption of the IMIM structure. (a) Dependence of top metal *Au* thickness. (b) Dependence of top metal material type. (c) Dependence of top insulator Si_3N_4 thickness. (d) Dependence of different types of top insulator material. (e) Plasmon resonance shift versus refractive index of top insulator. (f) Dependence of different types of bottom insulator material.

The planar analogue is used to analyze and understand the contributions from different material and structure parameters of nanopatterned IMIM architecture. Figure 4(a) shows absorption and reflection of the single planar and hexagonal nanopatterned *Au* layers. The average absorption of planar and nanopatterned layers is 27.7% and 47.3% respectively. This difference is explained by decreasing the reflectance of nanopatterned layer due to coupling of plasmon and optical cavity modes within pores, which leads to light absorption in metal inside the pore. The absorption widening is referred to different plasmon modes excited at variable metal width along *x* and *y* axes [m_0, m_1, and m_2, etc. in inset of Fig. 4(a)]. Figure 4(b) show that the absorption of single metal layer is increased by adding Al_2O_3 insulator and *Al* metal to the bottom of *Au* layer reaching 34.8% and 56.8% for planar MIM and nanopatterned MIM structures respectively. The enhancement of the absorption can be explained by the re-absorption of the light reflected by the bottom *Al* layer. Similar results for analogous MIM architectures were reported in [22–24]. Figure 4(c) illustrates absorption and reflection of single planar and hexagonal nanopatterned *Au* by adding the Si_3N_4 insulator. A large enhancement in absorption and widening of absorption spectrum are obtained due to decreasing of the strength of the surface plasmon resonance and thus higher electron energy lost through the its scattering [30]. The average absorption reaches 40.1% and 68.4% for planar and nanopatterned layers. The highest absorption is obtained for IMIM architecture, which is equal 46.5% for planar and 82.5% for nanopatterned layers as shown in Fig. 4(d). The enhancement absorption of *Al* at 650 nm is related to interband electron transition [32]. It should be noted that absorption inside *Al* is only around 5%, which is advantageous of using *Al* as bottom layer.

To further confirm the plasmon resonance shifting in the IMIM nanopatterned structure, which is induced by top insulator, the absorption profiles of IMIM architecture with different top insulator layers of SiO_2, Al_2O_3 and Si_3N_4 against pore radius and wavelength are simulated

#232636 - $15.00 USD Received 16 Jan 2015; revised 1 Mar 2015; accepted 30 Mar 2015; published 8 Apr 2015

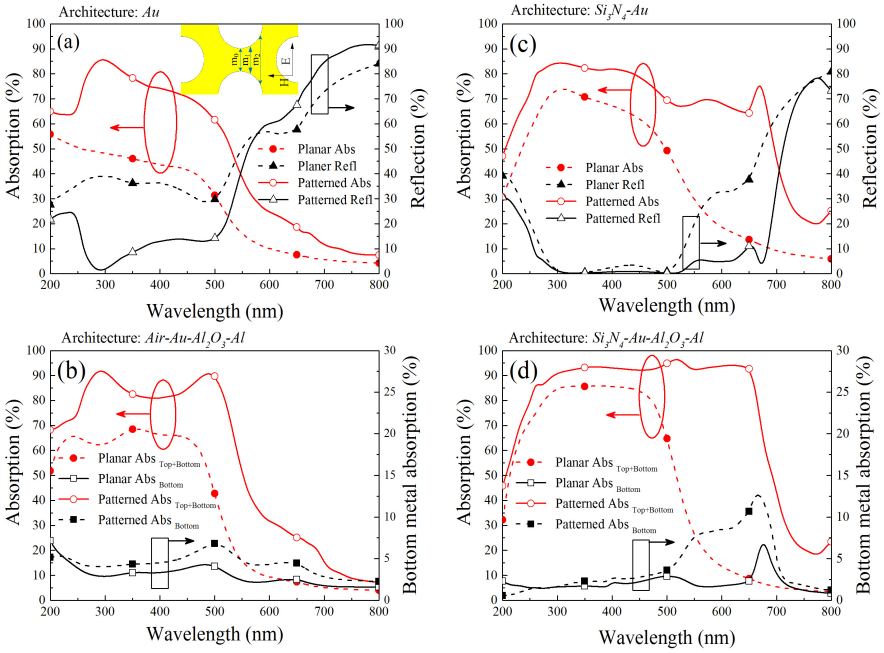

Fig. 4. Absorption and reflection dependency on the planar and hexagonal nanopatterned structures. (a) Absorption and reflection of *Au* single layer with planar and hexagonal structures. (b) Absorption of *air-Au-Al_2O_3-Al* planar and hexagonal structure and the corresponding absorption by the bottom *Al* layer. (c) Absorption and reflection of *Si_3N_4-Au* planar and hexagonal structure. (d) Absorption of planar *Si_3N_4-Au-Al_2O_3-Al* planar and hexagonal structure and the corresponding absorption by the bottom *Al* layer. For the nanopatterned IMIM structure parameters have r = 75 nm, d = 300 nm, w = 75 nm, $h_1 = h_2 = h_3 = h_4$ = 25 nm, $h_2 + w$ = 100 nm and *Si_3N_4-Au-Al_2O_3-Al* layers from top to bottom.

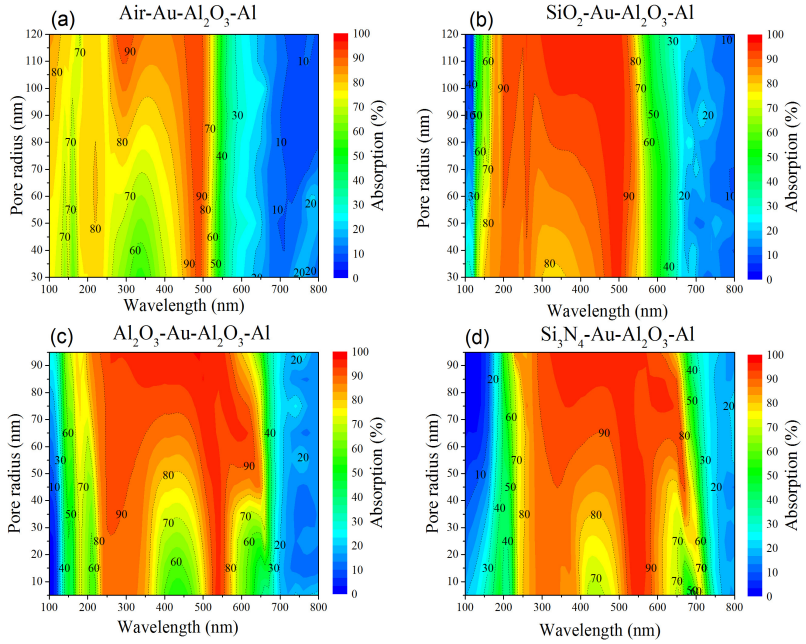

Fig. 5. Absorption profile of IMIM structure with top (a) *air*, (b) *SiO_2* (c), *Al_2O_3* and (d) *Si_3N_4* insulators versus pore radius and wavelength.

#232636 - $15.00 USD Received 16 Jan 2015; revised 1 Mar 2015; accepted 30 Mar 2015; published 8 Apr 2015

and shown in Fig. 5. It is can be seen that plasmon resonance shift happens even in large range of variation of pore radius.

In order to investigate the absorption spreading of incoming light in nanopatterned *Si_3N_4-Au-Al_2O_3-Al* structure, the two-dimension distribution of electric field intensity and light absorption profile along *y-z* plane are calculated for wavelengths close to absorption edge (350 and 650 nm) as demonstrated in Fig. 6. At wavelength of 350 nm, the electric field

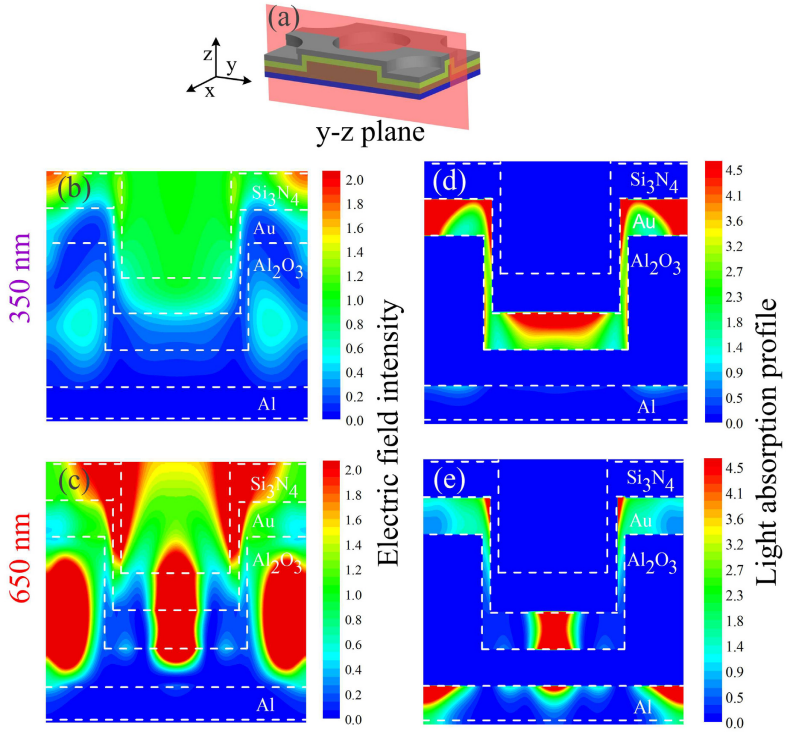

Fig. 6. Distribution of electric field intensity ($\left|E\right|^2 / \left|E_0\right|^2$) and light absorption profile (G/G_0) in nanopatterned *Si_3N_4-Au-Al_2O_3-Al* structure at the wavelengths of 350 and 650 nm. (a) Position of cross-section *y-z* plane (red plane) in above mentioned structure. (b, c) Electric field intensity distribution for 350 and 650 nm along *y-z* plane respectively. (d, e) Light absorption profile for 350 and 650 nm along *y-z* plane respectively.

intensity between top and bottom metals near the pore walls, which is due to coupling of plasmon and optical cavity modes [31]. The distribution peak of electric field intensity is being shifted to the central and top corner parts of pore at longer wavelength of 650 nm [Fig. 6(c)]. The enhancement of the electric field intensity between top and bottom layers provokes the growth of *Al* absorption from 7.5 to 12.5% for 650 nm [Fig. 4(c)]. Whereas, the light is absorbed with strong dependence on the distribution of the electric field intensity [Figs. 6(d) and 6(e)]: inside top metal layer with absorption maxima located where peaks of electric field intensity take place.

Finally, the absorption of IMIM structure versus incident light angle is shown in Fig. 7. Only slightly dropping is observed when the incident angle is from 35 to 70 degree. Small (<5%) difference of the absorption between TE and TM polarization over incident angle range from 0 to 90 degree.

#232636 - $15.00 USD Received 16 Jan 2015; revised 1 Mar 2015; accepted 30 Mar 2015; published 8 Apr 2015

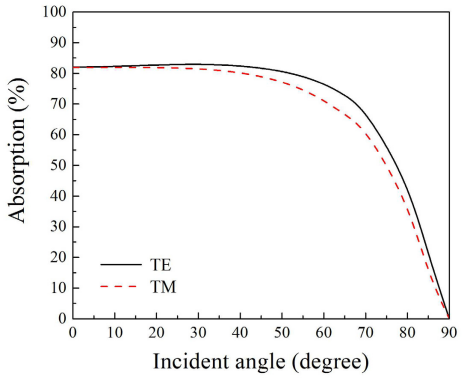

Fig. 7. Absorption profile of IMIM structure versus indecent light angle for the TE and TM polarizations.

4. Conclusion

A new polarization-independent light trapping architecture made of nanopatterned ultra-thin insulator-metal-insulator-metal (IMIM) architecture is designed and simulated. The IMIM structure is able to absorb of 82.5% of visible light in a broad wavelength range of 300 to 800 nm. The absorption of top metal layer is about 15.5 times of the bottom metal. Moreover, it shows weak incident angle dependence. The geometrical dimensions of IMIM design are optimized. It was found that by using different top insulator layer, the plasmon resonance response could be shifted more than 180 nm of wavelength in comparison with *air* (vacuum). The structure can be applied for plasmonic device applications with improved performance.

Acknowledgment

Financial support of National Research Foundation of Singapore (NRF7-CRP6-2010-2 and NRF-CRP12-2013-04).

#232636 - $15.00 USD Received 16 Jan 2015; revised 1 Mar 2015; accepted 30 Mar 2015; published 8 Apr 2015